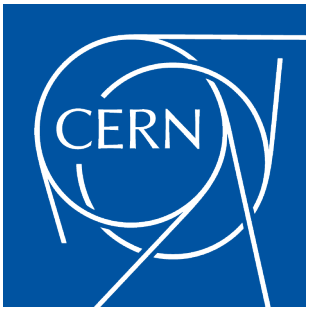

Computation of Optics Distortions due to Beam-Beam Interactions in the FCC-hh

Author : Patrik Gonçalves Jorge
Supervisor : Xavier Buffat

May 28, 2016

Computation of Optics Distortions due to Beam-Beam Interactions in the FCC-hh

Patrik Gonçalves Jorge

June 10, 2016

Contents

1 Introduction

Each beam in a collider consists in moving bunches composed of charged particles. Thus, an electromagnetic field is induced by these ensembles of moving charges and electromagnetic forces appear. These forces are very non-linear and may lead to various effects on the beam dynamics. For example, when two beams do not collide exactly head-on, the constant contribution from the force will change the orbit of the beam which may lead to a slightly different beam-beam effect and so on every turn.

Understanding these perturbations is crucial : large or underestimated perturbations can imply that particles constituting the beams may contact the elements of the accelerator. Given the amount of energy of these particles, non negligible damages to the electronics and to the superconducting magnets could be caused.

One of the solutions to prevent these issues is given by the system of collimators. Its aim is to protect the delicate elements of the machine, to help reduce the total dose on the accelerator equipment and to optimize the background for the experiments. It ensures in particular that the beam losses in superconducting magnets remain below quench limits. In order to clean the beams, specific insertions composed of collimators are dedicated to this function. This cleaning stage is achieved by placing very precisely blocks of materials close to the circulating beams, while respecting a predefined collimator hierarchy that ensures optimum cleaning in a multi-stage collimation process. The collimation hierarchy and therefore the cleaning efficiency is very sensitive to the machine optics, in particular to the β-function and the phase advance between collimators.

The simulations of this paper will be based on the Future Circular Hadron-Hadron Collider (FCC-hh) whose layout is presented in Fig. 1. The latter is a 100 km proton-proton collider project that planes to achieve a center-of-mass energy of 100 TeV. The accelerator is composed of two high-luminosity interaction points (IPA & IPG) and of two others with lower luminosity (IPH & IPF).

This paper will study the optics variations due to beam-beam interactions at IPA and IPG using computer simulations with MAD-X program. More specifically, it will concern firstly the influence of the phase advance between the two main interaction points with head-on collisions. Then, the impact on the optics of non-linear particles with head-on and long-range effects will be studied.

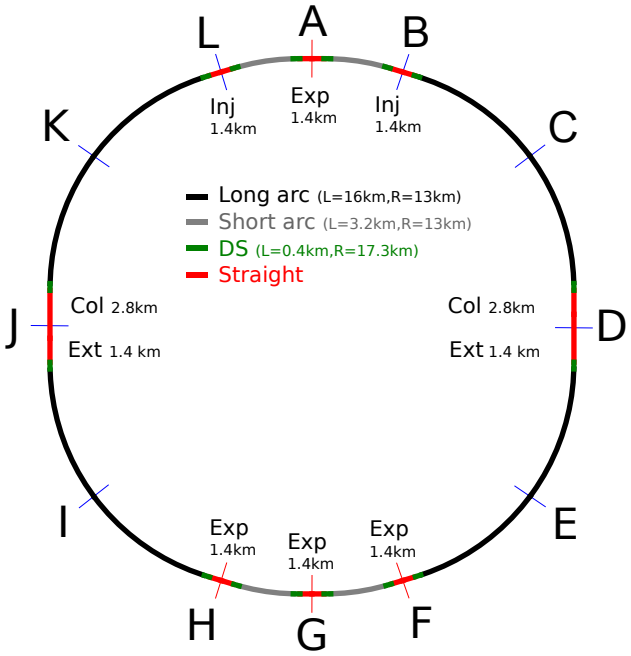

Figure 1: Layout of the FCC

2 Theoretical approach

2.1 Beam-beam interaction

2.1.1 Head-on interactions

A head-on beam-beam collision induces a force on the particles crossing each other. One can express the radial force for a Gaussian beam distribution on a particle [1] :

$$F_r(r) = -\frac{nq^2(1+\beta^2)}{2\pi\epsilon_0}\frac{1}{r}\left[1-\exp\left(-\frac{r^2}{2\sigma^2}\right)\right] \tag{1}$$

where n is the line density of particles in the beam, ϵ_0 the vacuum permittivity and β corresponds to the normalized speed of the particles. Note that for small amplitudes (i.e. below $\approx 1\sigma$), the force is approximately linear which means that the particles traveling see the beam coming from the opposite direction as a defocusing quadrupole when they are close enough to the beam center.

This interaction will induce a change in the β-function all along the accelerator. Considering small amplitudes, one can derive analytically the change of the β-function coming from N small quadrupole errors (i.e. head-on collisions at small amplitudes) at positions s_i $(i = 1, ..., N)$ [3] :

$$\frac{\Delta\beta(s)}{\beta_0(s)} = \frac{2\pi\xi}{\sin(2\pi Q_0)}\sum_{i=1}^{N}\cos(2|\mu_0(s)-\mu_0(s_i)|-2\pi Q_0) \tag{2}$$

2.1.2 Long-range interactions

The FCC-hh aims to collide bunches of particles of the same type against each other like the LHC. This implies that the bunches of particles that compose the beam must travel in separate beam pipes. Collisions are then induced by making the beams cross using separation and recombination magnets : bunches will finally collide at a small crossing angle. At this stage, one can distinguish two kinds of interactions acting on the bunches of particles : head-on and long-range interactions (Fig. 2). Head-on interactions concern the interactions between bunches colliding quasi head-on at the center (Sec. 2.1.1). The other bunches that are kept separated by the crossing angle and that feel the electromagnetic forces from the opposite beam are affected by long-range interactions. Fig. 2 illustrates these two types of interactions at the collision region. The large number of long-range interactions and some of their properties imply that this kind of interactions are important even if they distort the beams much less than head-on collisions.

Among the effects introduced by long-range interactions, one can mention the opposite sign of the tune shift. This can easily be understood by using the plot of the derivative of the radial force exerted on a particle given by Eq. 1 (Fig. 3). The tune shift of a particle is then obtained by averaging the slope of the force over the range of the particle's oscillation

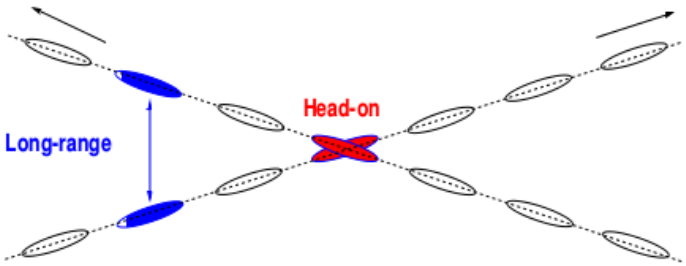

Figure 2: Head-on and long-range interactions at an interaction point [1]

amplitude.

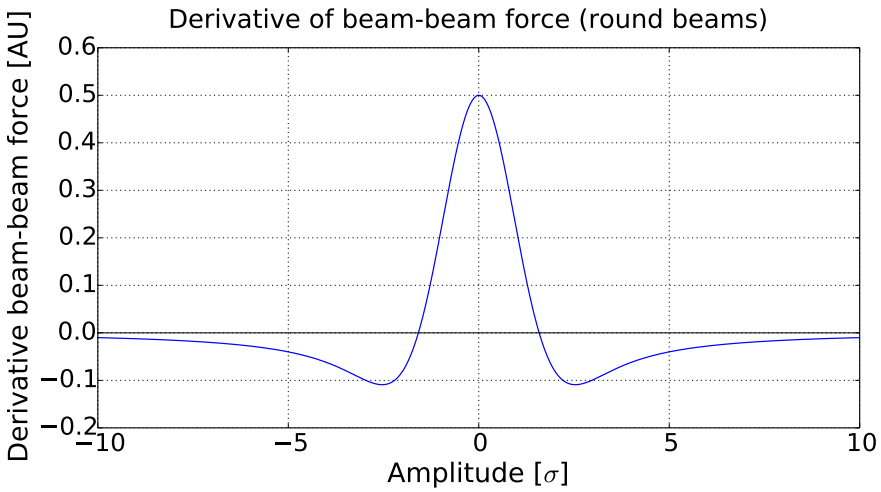

Figure 3: Derivative of beam-beam force for round beams (Eq. 1)

When one averages the value of the derivative over the range of a particle, one should keep in mind that the force (and its derivative) represented in Fig. 3 correspond to the one induced by the other beam. Since the slope of the force becomes negative for amplitudes larger than $\approx 1.5\sigma$, the resulting tune shift for long-range interactions (typical separation is about 7σ and 10σ) will have the opposite sign with respect to a head-on collision (i.e. close to amplitude zero where the slope is positive).

2.2 Analysis of tracking data

2.2.1 Singular Value Decomposition

The Singular Value Decomposition (SVD) corresponds to the factorization of a matrix and can be seen as the generalization of the eigendecomposition of a positive semidefinite normal matrix.

Let $\mathbf{M}$ be a $m \times n$ matrix whose coefficients are real or complex. Formally, the singular value decomposition of $\mathbf{M}$ is a factorization of the form [4] :

$$\mathbf{M} = \mathbf{U}\mathbf{\Sigma}\mathbf{V}^* \tag{3}$$

where $\mathbf{U}$ is a $m \times m$ unitary matrix, $\mathbf{V}^*$ is the conjugate transpose of $\mathbf{V}$ which is a $n \times n$ unitary matrix and $\mathbf{\Sigma}$ is a $m \times n$ diagonal matrix whose diagonal coefficients are positive reals (singular values of $\mathbf{M}$). By convention, the singular values $\sigma_1, ..., \sigma_m$ are listed in descending order in matrix $\mathbf{\Sigma}$.

Matrices from the SVD factorization can provide informations about the β-function and α-function through Floquet transformation. The Floquet transformation is defined by the coordinate transformation [5] :

$$\begin{pmatrix} u \\ u' \end{pmatrix} = \underbrace{\begin{pmatrix} \beta^{1/2} & 0 \\ -\alpha\beta^{-1/2} & \beta^{-1/2} \end{pmatrix}}_{\mathbf{F}} \cdot \begin{pmatrix} \eta_u \\ \eta'_u \end{pmatrix} \tag{4}$$

where η and η' are called Floquet or Courant-Snyder coordinates. This transformation reduces the betatron oscillation solution to the form of a simple harmonic oscillator solution. Indeed, whereas the trajectory of the particle in phase space (u, u'), where $u = x, y$, is defined by an ellipse, the new variables (η_u, η'_u) change this ellipse into a circle in the new coordinate system. Therefore, after the transformation to the new variables $\{u, s\} \rightarrow \{\eta, \phi\}$, the solution takes the simple form [5] :

$$\eta_u(\phi) = A\cos(Q_u\phi + \phi_0) \tag{5}$$

where Q_u is the tune in the respective plane and $Q\phi$ the phase angle of the oscillation. One can make the link between the SVD factorization and the Floquet transformation : let us consider $\mathbf{M}$ as being a $2 \times N$ matrix where each column is a pair (u, u') of a particle and where N is the number of points in phase space at a certain location s (i.e. number of turns). Therefore, the SVD will decompose $\mathbf{M}$ into three matrices as follow :

$$\begin{pmatrix} u_1 & ... & u_N \\ u'_1 & ... & u'_N \end{pmatrix} = \begin{pmatrix} U_{11} & U_{12} \\ U_{21} & U_{22} \end{pmatrix} \cdot \begin{pmatrix} \sigma_1 & 0 & 0 & ... & 0 \\ 0 & \sigma_2 & 0 & ... & 0 \end{pmatrix} \cdot \begin{pmatrix} V^*_{11} & ... & V^*_{1N} \\ \vdots & & \vdots \\ V^*_{N1} & ... & V^*_{NN} \end{pmatrix} \tag{6}$$

The link between the SVD and the Floquet transformation can be made if one takes the product of the matrices $\mathbf{U}$ and $\mathbf{\Sigma}$ (only its 2 non-zero first columns). This product is then equivalent to the transformation matrix $\mathbf{F}$ in Eq. 4 that transforms the phase space coordinates (u, u') into the Floquet ones : each point in phase space (u_i, u'_i) where $i = 1, 2, ..., N$ contributes to the same ellipse and therefore to the same α-function and β-function :

$$\mathbf{F} = \begin{pmatrix} \beta^{1/2} & 0 \\ -\alpha\beta^{-1/2} & \beta^{-1/2} \end{pmatrix} \sim \begin{pmatrix} U_{11} & U_{12} \\ U_{21} & U_{22} \end{pmatrix} \cdot \begin{pmatrix} \sigma_1 & 0 \\ 0 & \sigma_2 \end{pmatrix} = \begin{pmatrix} \sigma_1 U_{11} & \sigma_2 U_{12} \\ \sigma_1 U_{21} & \sigma_1 U_{22} \end{pmatrix} = \mathbf{S} \tag{7}$$

To sum up, Floquet transformation results in a change of coordinates such that the ellipse in phase space becomes a circle exactly like the SVD does. However, the basis of the matrices $\mathbf{F}$ and $\mathbf{S}$ are not necessarily the same even if their effect is the same. Indeed, if one takes a circle in a certain basis and rotates the basis, the circle will remain a circle while the basis is different. This means that before comparing both transformation matrices ($\mathbf{F}$ and $\mathbf{S}$), one of them should be transformed by rotating its basis (i.e. compute $\mathbf{RSR^{-1}}$ where $\mathbf{R}$ is the rotation matrix in $\mathbb{R}_2$). This way, one can be sure that the basis (and so the form) of the SVD matrix $\mathbf{S}$ is the same as the one of the Floquet transformation $\mathbf{F}$: the top right component is zero and the product of the diagonal components is equal to 1.

Finally, since the singular values are listed in descending order by convention, the way the ellipse looks like (horizontal or vertical) is not necessarily conserved : the ellipse may be reversed with respect to one of its axis such that a flip of the axis besides the previous rotation $\mathbf{R}$ may be needed.

2.2.2 Tracking with MAD-X

The non-linearity of the particles often leads to a reduction of the available dynamic aperture. The latter defines the phase space region in which the beam remains stable. Particles are usually lost when they have reached large amplitudes and when they bit the physical aperture. In the real machine, this is observed by the measurement of particle losses and a reduced beam life time.

Since the equations of motion are non-linear, the most efficient way to get informations about beam stability and dynamic aperture/acceptance is to perform numerical particle tracking studies.

Tracking programs essentially follow single particles along their path incorporating any nonlinear field encountered : the deflections of all non-linearities encountered are accumulated for a large number of turns and beam stability or instability is judged by the particle surviving the tracking (i.e. its amplitude stays within some limits) or not, respectively. Since the diffusion mechanisms due to the non-linearities are usually slow, such simulations must be performed on a large number of turns ($\sim 10^6$ in the case of the LHC).

The main difference between tracking procedure and a twiss (used last semester [6]) is that the evolution of the particle is deduced using maps and not matrices any more. The mapping of the particle vector $X = (x, x', y, y', \delta, \Delta s)$ from one turn to the next ($X^n \xrightarrow{map} X^{n+1}$) with the order of the map corresponding to the highest power in the coordinates can be used to calculate the one-turn map. Thus the closed orbit is a fix point of the one-turn map. [1]

Note that the procedure of tracking in MAD-X is done using thin lenses, meaning that a lattice defined with thick elements has to be converted first before the tracking. With thin lenses, the effects of an element (e.g. a quadrupole) on the beam can be represented as impulses (kicks) at the positions of the thin elements, which simplifies the treatment. This method is very fast and symplectic by construction and it is therefore best suited for particle tracking. [2]

Let's illustrate the tracking procedure done with MAD-X and the SVD factorization (Sec. 2.2.1). Fig. 4 shows the Poincarré section of a particle in phase space at a bending magnets (called MB1). The particle describes a tilted ellipse in phase space due its large α value ($\alpha_x = 2.55$) as expected. From this Poincarré section, the SVD allows to make a transformation equivalent to the Floquet one on the ellipse and thus changes it into a circle (Fig. 5). The deviation of the points describing the particle in Floquet space coordinates with respect to the fitted circle is very small : $\Delta r/r_c < 1\%$ where r_c corresponds to the radius of the fitted circle, meaning that the SVD procedure as a Floquet transformation works (with a very small deviation from theoretical predictions) and may provide correct results about the optics parameters.

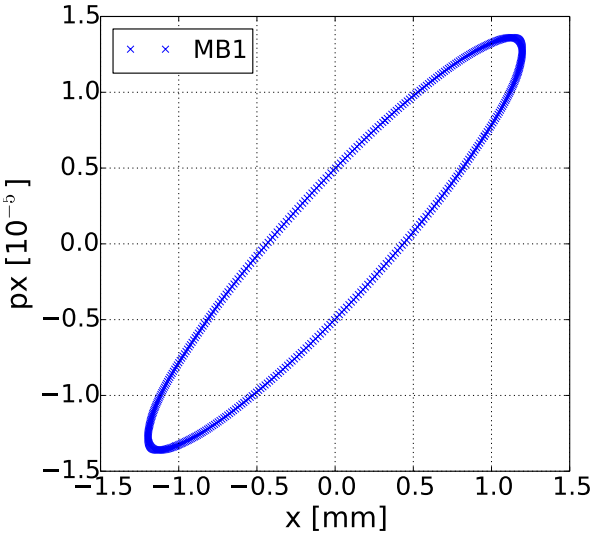

Figure 4: Poincarré section of a particle with amplitude $12\sigma_x$ in horizontal plane at bending magnet MB1

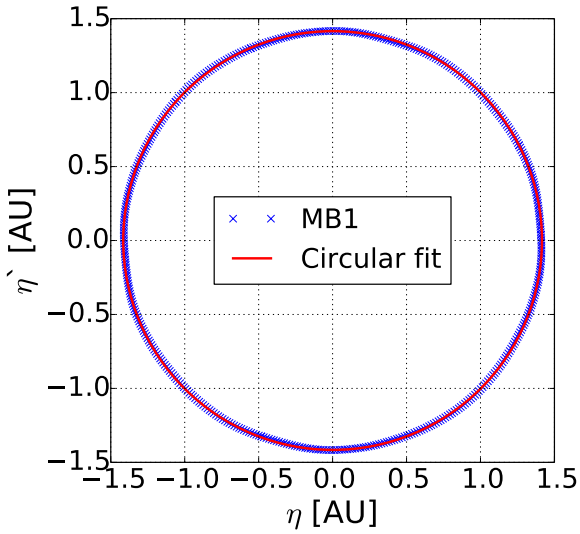

Figure 5: Floquet transformation of betatron oscillations from Fig. 4 using SVD and related circular fit

2.2.3 Tunes Footprint

Let us now consider particles oscillating at large amplitude. In order to understand the effect of the amplitude of the particle on the tune after a head-on collision, it is suitable to look at the derivative of the radial force exerted on a particle given by Eq. 1 (Fig. 3). As said previously, the tune shift of a particle is obtained by averaging the slope of the force over the range of the particle's oscillation amplitude.

One sees on Fig. 3 that, on the one hand, particles with small amplitudes ($< 0.5\sigma$) have the largest tune shift and that, on the other hand, particles with large amplitudes ($> 3\sigma$) have a smaller tune shift due to the negative part of the derivative of the force. One can even prove that the tune shift of particles with extremely large amplitudes tends theoretically to zero since the integral of the derivative of the force (i.e. the force) tends to zero for infinite amplitudes.

In a 2-dimensional case, the tune shifts on both planes of a particle with amplitudes x

and y depend on both, horizontal and vertical amplitudes. In order to present this detuning, a 2-dimensional form called tune footprint is normally preferred : the amplitudes (x,y) are mapped into the tune space (Q_x,Q_y). Some tune footprints of the FCC-hh are presented in Fig. 6 and 7. The blue dot represents the initial tunes ($Q_{x,0}, Q_{y,0}$)=(0.31, 0.32) of the machine without any collisions.

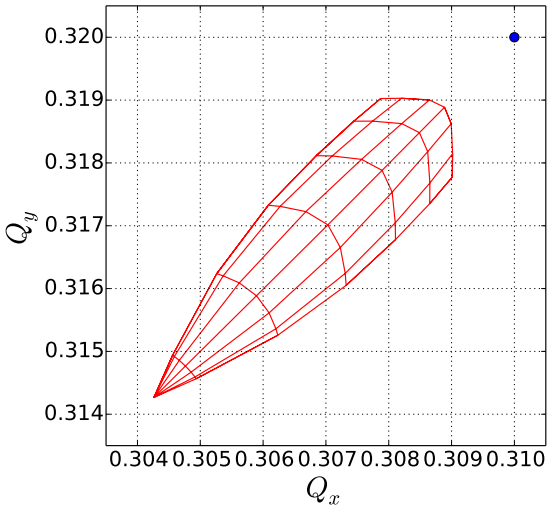

Figure 6: Tune footprint for two head-on collisions at IPA & IPG. Vertical and horizontal amplitudes are between 0 and 6σ.

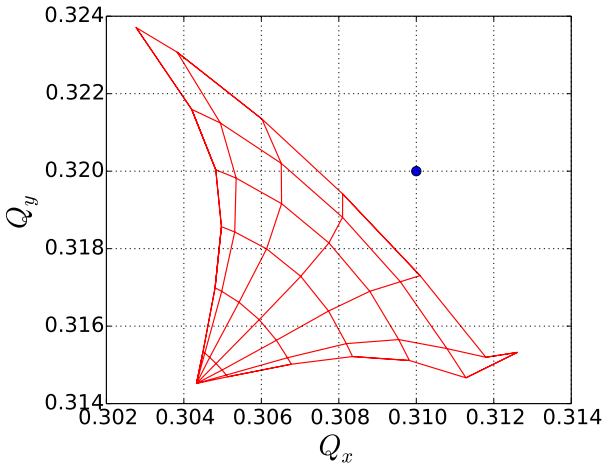

Figure 7: Tune footprint considering head-on and long-range interactions at IPA & IPG. Vertical and horizontal amplitudes are between 0 and 6σ.

The footprint given in Fig. 6 is the one for two head-on collisions at IPA and IPG. We see that the furthest detuning is reached for small amplitude and that as the amplitude increases, the tune gets closer and closer to the initial one as expected.

When one takes into account long-range interactions (Fig. 7), the tune footprint is totally different and the spread in particle tunes increases. The new tunes at small amplitudes remain the same, however, the bigger are the amplitudes, the further we are from the initial tunes : the large amplitude particles experience the strongest long-range beam-beam perturbations. This is rather intuitive since the particles with the largest amplitudes are the ones that get the closest to the opposing beam. Thus, when one takes into account long-range interactions, the area covered in tune space enlarges and the chance to cross a resonance and to lose the particle becomes bigger.

Note that an artefact can be noticed at the lower right corner amplitude on Fig. 7 : the latter comes from the fact that the detuning is so large that the particle crosses the line where $Q_x = Q_y$. This induces then an error in the deduction of the tunes in the frequency spectrum of the particle since both peaks are very close to each other.

Finally, it can be shown that the tune footprint in Fig. 7 is a combination of the effects of the different kinds of interactions (head-on & long-range) from each interaction point (IPA & IPG).

3 Simulations and discussion

The results can be divided into two main parts : first, the study of the effect of the phase advance μ between the two main interaction points (IPA & IPG) on the β-function and secondly, the calculation of the β-function and α-function obtained by particle tracking and SVD considering head-on and long-range interactions respectively.

3.1 Effect of the phase advance between two interaction points

The original configuration of the accelerator is symmetric with respect to the phase advance between the two main interaction points IPA and IPG ($\Delta\mu_{A\to G} = \Delta\mu_{G\to A}$). It is however possible to break this symmetry by introducing phase advance shifts on both sides of the ring (right-hand side for A→G and left-hand side for G→A as in Fig. 1).

The insertions F and H have been used to create this phase advance shift. These insertions are reserved for potential physics experiments but for the purpose of our study, they might be rematched with different phase advances the following way : one should increase the value of the phase advance by $\Delta\mu$ (in both planes compared to its original value) between the beginning of the insertion F and its end by changing the strength of some quadrupoles within this insertion. In addition, the twiss parameters must remain the same at the entrance and at the end of each insertion. This last condition implies that the beam evolution will remain unchanged outside the insertions, meaning that the phase advance at IPG and at the beginning of the insertion H will be also shifted by $\Delta\mu$ compared to its original value. The second step is almost identical to the first one : the insertion is now H and the sign of the phase advance shift is different. Thus, the tune is conserved after both phase advance shifts. In conclusion, the phase advances between IPA and IPG will be : $\mu_{A\to G} = \mu_{sym} + \Delta\mu$ and $\mu_{G\to A} = \mu_{sym} - \Delta\mu$, where μ_{sym} corresponds to half of the total phase advance.

Physically, this change in the phase advances between both interaction points will lead to a change in the β-beating due to beam-beam interactions as in Eq. 2 where the phase advances of both quadrupole errors appear in the absolute value.

Following the procedure described above, the maximum of the β-beating due to two head-on collisions at IPA and IPG has been calculated using MAD-X varying the phase advance shift $\Delta\mu$ (Fig. 8).

The maximum of the β-beating in both planes has the same periodicity. The similarity in the maximum value comes from the tunes of both planes (Q_x and Q_y) on which the β-beating depends (Eq. 2) and thus its maximum. The maximum of the β-beating will be also π-periodic for any tunes with respect to $\Delta\mu$ given the Eq. 2 where the phase advance appears in the absolute value inside the cosine function.

Thus, it is possible to control the maximum of the β-beating in one plane by choosing the phase advance shift to introduce in the beam. We can put the accelerator in different configurations such that the beating is the same in both planes or very different. For

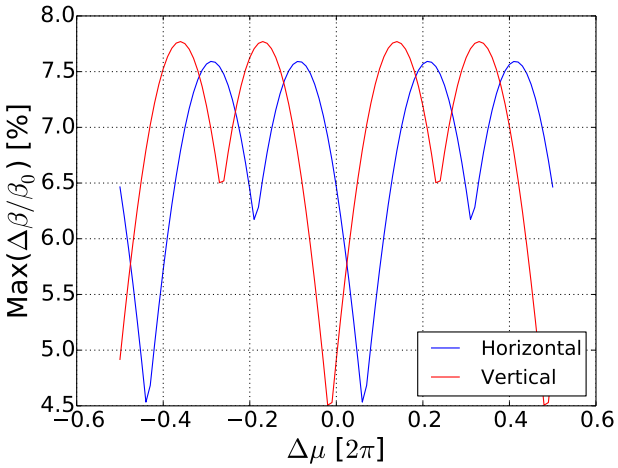

Figure 8: Maximum of the β-beating as a function of the phase advance shift $\Delta\mu$ between IPA&IPG

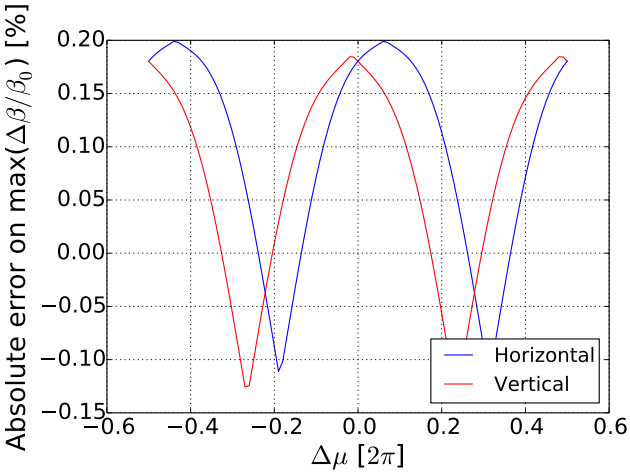

Figure 9: Absolute error of the maximum of the β-beating between the β-beating from Fig. 8 and the one from Eq. 2

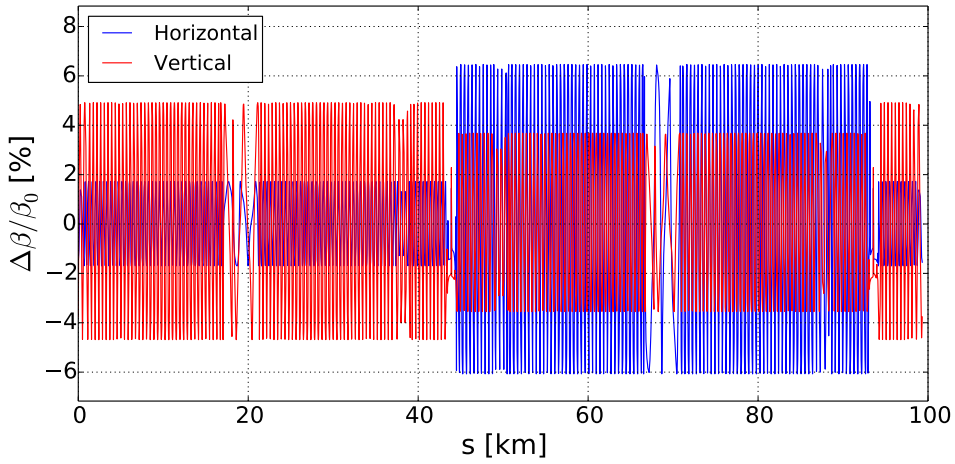

Figure 10: β-beating in the FCC-hh with two head-on beam-beam interactions at IPA ($s \approx 45$ km) and IPG ($s \approx 95$ km) for the original tunes ($Q_x = 108.31$ and $Q_y = 108.32$)

example, the original configuration ($\Delta\mu = 0$) is not symmetric relatively to both planes and for $\Delta\mu \approx 0.06$, the maximum of the β-beating on the horizontal plane is about 4.5% and the one on the vertical plane is approximately 7%. However, there exists some configurations where the maximum of the β-beating is equal in both planes.

The comparison between the results provided by MAD-X and the expected theoretical maximum β-beating from Eq. 2 is presented in Fig. 9. The absolute error between the optics from the simulations and the formula with two quadrupole errors is also periodic and remains under 0.2% for every $\Delta\mu$ which shows that Eq. 2 models in a satisfactory way the physical effects on the beams due to the two head-on collisions.

The study of the influence of the initial tune Q_0 on the envelope of the β-beating has showed that the envelopes described by the maximum of the β-beating between each interaction points varies with respect to the value of Q_0 in both planes ([6]). Fig. 10 illustrates

the notion of envelope whose amplitude changes depending on which side of the accelerator we are : right-hand side (IPA→IPG) or left-hand side (IPG→IPA). The same applies to the phase advance shift $\Delta\mu$ between each interaction point (Fig. 11).

Fig. 11 represents the maximum of the β-beating as a function of the phase advance shift $\Delta\mu$ for each side of the ring. The maximum of the β-beating in one plane can be very different depending on which side of the ring we are considering. There are extreme cases where the maximum of the β-beating is close to zero on one side and near its maximum on the other side for both planes (for example $\Delta\mu \approx 0.39$ for vertical plane and $\Delta\mu \approx 0.16$ for horizontal plane). Consequently, this phenomenon should be taken into account in the development of the collimation system : if one assumes that the collimation system will be located only on one side of the ring, it may not be able to clean the beams efficiently.

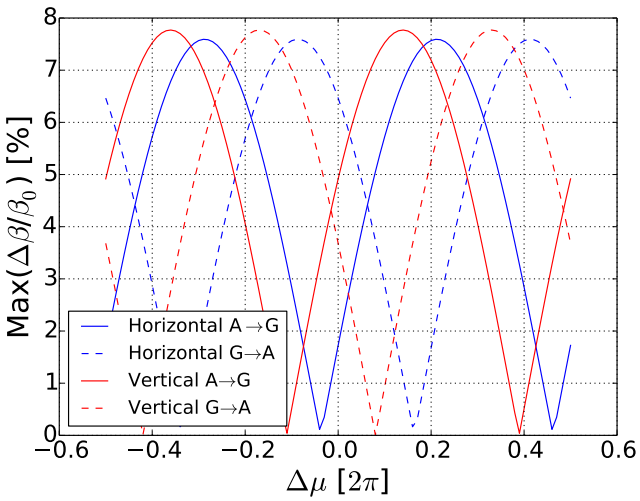

Figure 11: Maximum of the β-beating between A&G (right-hand side of the ring) and G&A (left-hand side)

3.2 Phase space and β-function calculation

We are now going to investigate the phase space and its transformations in order to extract some variables such as the β-function. All the simulations that follow have been made for a representative set of elements in the ring : the two main interaction points (IPA & IPG), four focusing/defocusing quadrupoles (QF & QD) and four bending magnets (MB). The dipoles and quadrupoles have been taken according to their phase advance (Tab. 1).

	IPA	IPG	QF1	QF2	QF3	QF4
μ_x	0	0.2960	0.5210	0.1444	0.4267	0.0511

	QD1	QD2	QD3	QD4	MB1	MB2	MB3	MB4
μ_x	0.6435	0.2674	0.3012	0.9277	0.8638	0.7966	0.7899	0.0412

Table 1: Phase advance (modulo 2π) in horizontal plane for each element with respect to IPA

The study has been made on the horizontal plane : the amplitude of the particles used in the tracking procedure were along the x-axis and homogeneously distributed from $0.05\sigma_x$ to

$12\sigma_x$. Finally, the simulations have been done using the SVD (Sec. 2.2.1) and the particle tracking (Sec. 2.2.2) for a total number of 5000 turns in the ring for each particle.

3.2.1 Head-on interactions

Let's first consider head-on collisions at both interaction points.

In the case of a particle with amplitude approaching zero, one expects the change in the β_x-function to become equal to the one introduced in [6] (called β_{twiss} from now on) since the particle in the twiss was on the central axis with very small perturbations.

However, in the case where the amplitude of the particle tends to infinity, one would expect that the $\Delta\beta_x$ induced after the two collisions gets smaller and smaller as the amplitude of the particle gets larger. Indeed, as discussed in Sec. 2.2.3, the tune shift tends to zero when the amplitude of the particle become very large in a head-on collision. Using Eq. 2, one can deduce the effect on the β-function : for small values of the beam-beam parameter ξ and a tune far enough away from linear resonances this parameter is equal to ΔQ such that the β-beating is actually proportional to the tune shift.

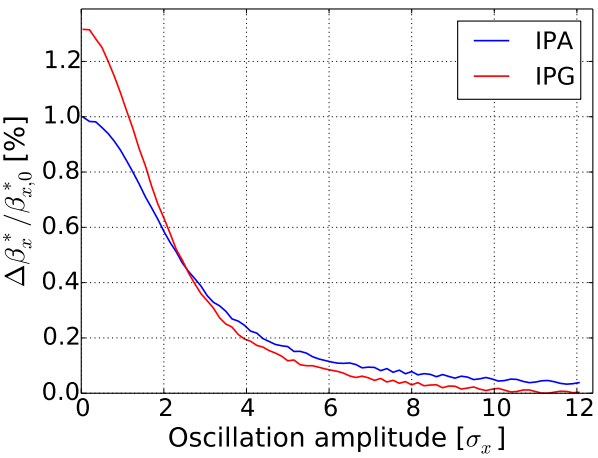

Figure 12: β-beating of a particle as a function of its oscillation amplitude at both interaction points for two head-on collisions

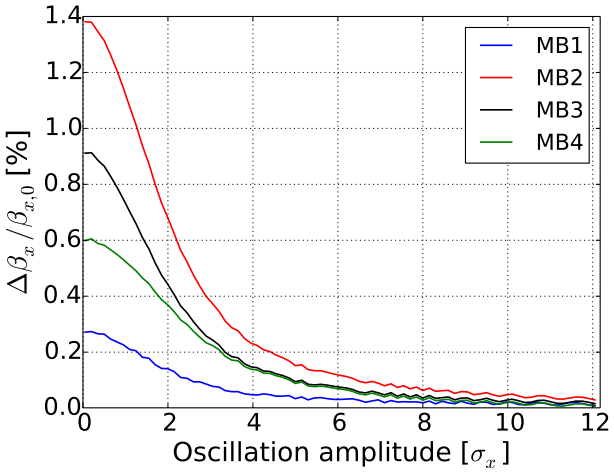

Figure 13: β-beating of a particle as a function of its oscillation amplitude at the four bending magnets for two head-on collisions

The β-beating relatively to the value of the β-function without the two collisions $\beta_{x,0}$ are given in Fig. 12, 13, 14 and 15 for all the elements. As one can see, the shape of the curves are rather smooth with a little bit of numerical noise, showing that the calculation process of the β-function with the SVD method may provide workable and physical outcome. Increasing the number of turns for each particle may reduce this numerical noise.

Concerning the limit values of the β-beating, one can see that it seems to tend to zero in all the cases as expected when the amplitude is large as in the tune footprint (Fig. 6). It has also been verified that the particles with small amplitudes have a β-beating that is close to β_{twiss}. The relative difference between the value of the β-function at the largest

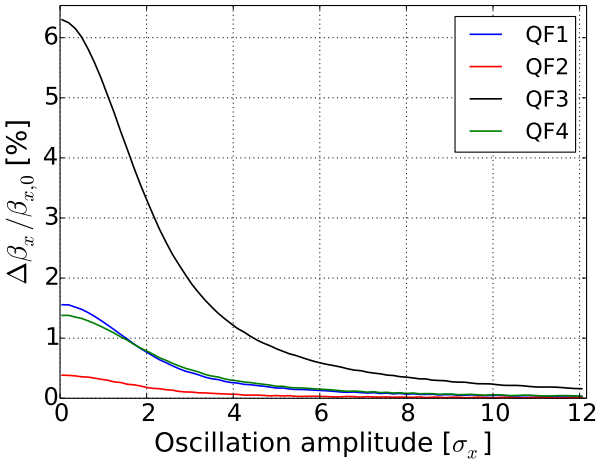

Figure 14: β-beating of a particle as a function of its oscillation amplitude at the four focusing quadrupoles for two head-on collisions

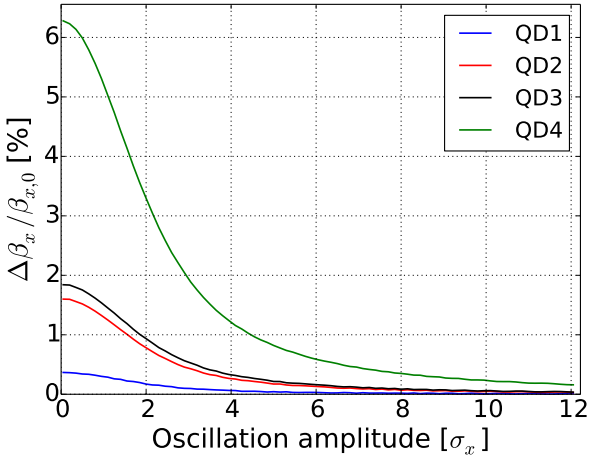

Figure 15: β-beating of a particle as a function of its oscillation amplitude at the four defocusing quadrupoles for two head-on collisions

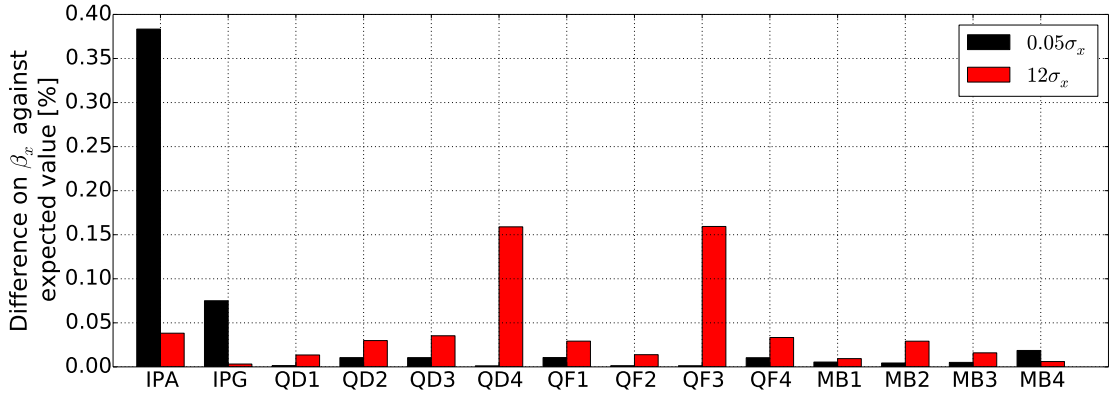

Figure 16: Difference on β_x at $0.05\sigma_x$ and $12\sigma_x$ from Fig. 12, 13, 14 and 15 against the expected values

amplitude ($12\sigma_x$) and $\beta_{x,0}$ as well as the difference between the value of the β-function at the smallest amplitude ($0.05\sigma_x$) and β_{twiss} is presented in the histogram in Fig. 16 in order to clearly appreciate the deviations from the expected values.

All the differences against the expected value remain under 0.4% which is satisfactory. The large majority of the comparisons are even more encouraging : the difference stands under 0.05%. Increase the largest amplitude of the particle in the tracking and decrease the smallest one should permit to obtain even better results and therefore get closer to the expected values.

The SVD also permitted to extract informations about the α-function since it appears in the transformation matrix $\mathbf{F}$ of the Floquet transformation (Eq. 4). The same reasoning can be made here as for the β-function about the limit values of the α-beating at small and large amplitudes. However, only the results for bending magnets are presented below since the α_x is zero at the interaction points and at the quadrupoles of a FODO lattice. The

α-beating and the difference against the expected values are presented in Fig. 17 and 18.

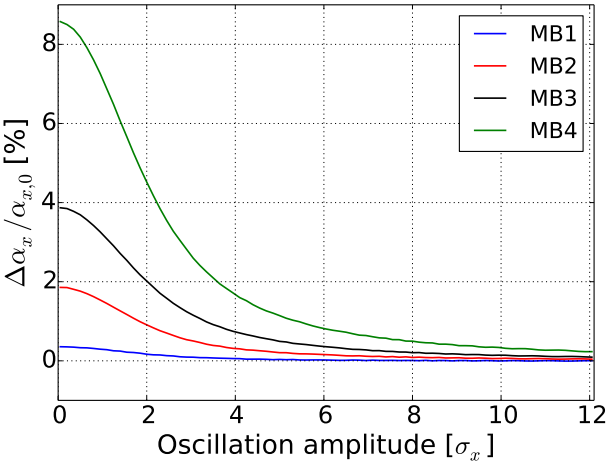

Figure 17: α-beating of a particle as a function of its oscillation amplitude at the four bending magnets for two head-on collisions

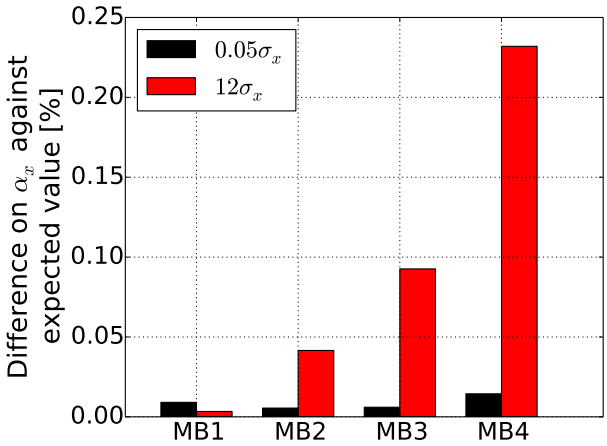

Figure 18: Difference on α_x at $0.05\sigma_x$ and $12\sigma_x$ from Fig. 17 against the expected values

One sees on Fig. 17 that the curves are relatively similar to the ones for the β-beating. The α_x-function tends to zero for all the elements at large amplitude and tends to a certain value of α-beating for very small amplitudes. Fig. 18 shows that the difference remains under 0.25% at $12\sigma_x$ with respect to zero and that for the smallest amplitude ($0.05\sigma_x$), the value is even closer to α_{twiss} : the difference remains under 0.016%.

3.2.2 Head-on & long range interactions

Let's now consider collisions where head-on and long-range interactions are taken into account (Sec. 2.1.1 & 2.1.2) at both interaction points. Thanks to particle tracking performed by MAD-X and the SVD procedure, one has been able to extract the value of the β_x-function at each observation points.

The β-beating for all the different elements is given in Fig. 19, 20, 21 and 22. As one can see, the results are very different from the ones obtained in the case with head-on interactions in Sec. 3.2.1. Indeed, the value of the β-beating at small and large amplitude are different, the shape of the curves describing the β-beating isn't the same and finally, there seems to be an amplitude from which the β-function extracted from the SVD becomes very irregular for all the elements.

Concerning large amplitudes, the β-beating fluctuates a lot and doesn't approach zero in any cases as in head-on collisions. This result is coherent with the tune footprint taking into account long-range interactions (Fig. 7) : the tune shift (and therefore the β-beating) isn't going to zero for large amplitudes either.

Then, the value of the β-beating for the particle with the smallest amplitude ($0.05\sigma_x$) is generally greater to the one in Sec. 3.2.1 with only head-on interactions. This difference is

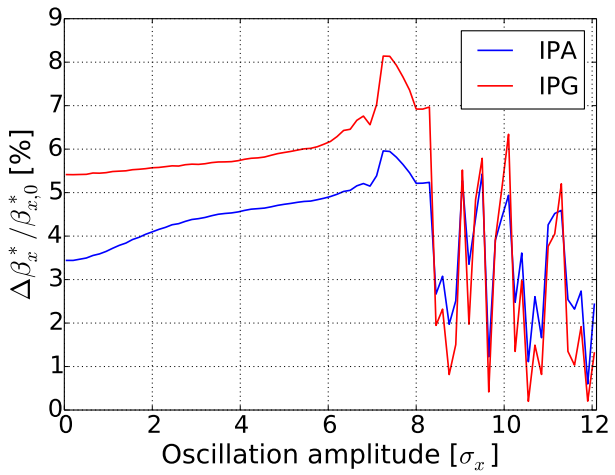

Figure 19: β-beating of a particle as a function of its oscillation amplitude at both interaction points for head-on & long-range interactions

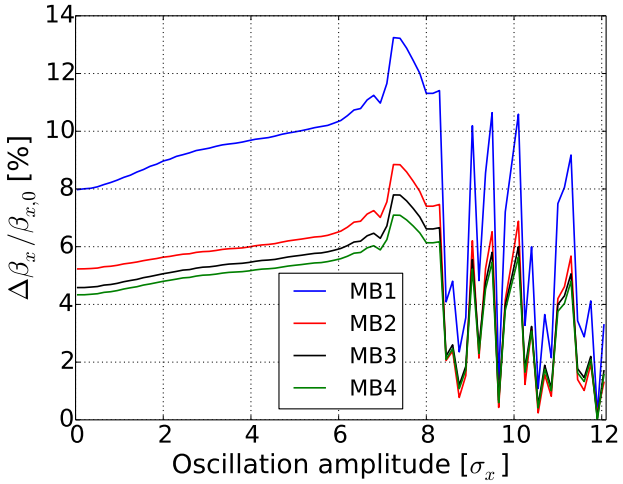

Figure 20: β-beating of a particle as a function of its oscillation amplitude at the four bending magnets for head-on & long-range interactions

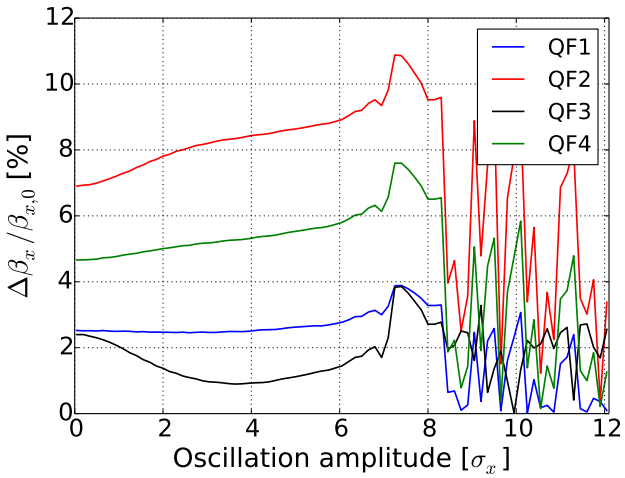

Figure 21: β-beating of a particle as a function of its oscillation amplitude at the four focusing quadrupoles for head-on & long-range interactions

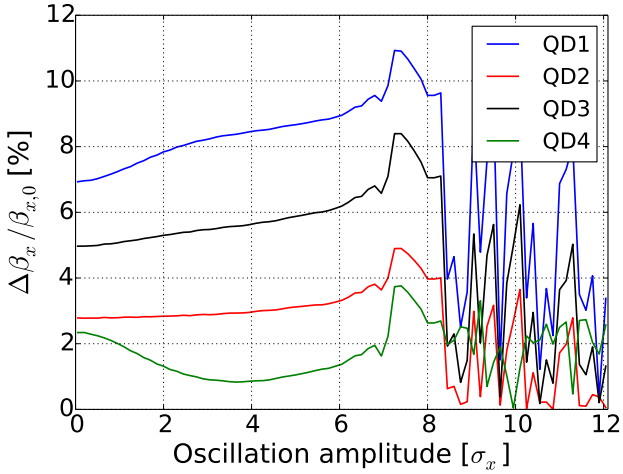

Figure 22: β-beating of a particle as a function of its oscillation amplitude at the four defocusing quadrupoles for head-on & long-range interactions

due to the fact that the interactions taken into account are not the same : in one case, only head-on collisions were considered and in the present one, both head-on and long-range interactions are taken into account.

Fig. 23 permits to to clearly observe the difference between this case and the previous one by showing the deviation of the value of the β-function with respect to the the expected values (chosen the same way as in head-on case) at both maximum and minimum amplitude of the tracking simulations. As one can see, the differences against the β-function at large amplitude are generally big compared to head-on collisions. Concerning the values of the β-function at small amplitude, the difference remains under 0.04% which shows that the SVD method works fine for this range of amplitude.

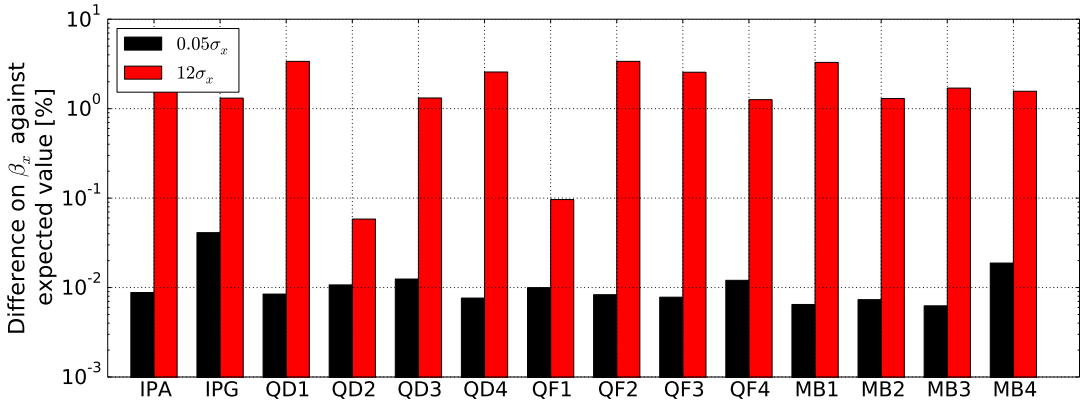

Figure 23: Difference on β_x at $0.05\sigma_x$ and $12\sigma_x$ from Fig. 19, 20, 21 and 22 against the expected values

The irregularity of the results obtained for large amplitude suggest that the model is no longer appropriate for particles motion. The presence of chaotic motion due to strong non linearities induced by long-range beam-beam interactions does not allow to define an invariant of motion and therefore the values of the β-function obtained with this method are meaningless. Note that a logarithmic scale has been used in Fig. 23 because of the different scales of the deviations between 12σ and 0.05σ.

Let's study the phase space and the Floquet transformation in order to understand the behaviour of the results for amplitudes from $8.3\sigma_x$. Firstly, it has been observed that for amplitudes $\leq 5\sigma_x$, the particle described in phase space a trajectory very similar to the one presented in Fig. 4. After the Floquet transformation, the trajectory was therefore very close to a circle like in Fig. 5. For particles with an amplitude greater than $\sim 5\sigma_x$, the phase space ellipse begins to become irregular in the distribution of the points and slightly deformed (Fig. 24). The circle after Floquet transformation starts then to distort and approach the geometric shape of a triangle until $8.3\sigma_x$ (Fig. 25). The circular fit begins to be non-consistent with the provided results.

From $8.3\sigma_x$, all the values of the β-beating start to become irregular and non-continuous. The reason for this change can be found in Fig. 26 and 27. As one can see, the ellipse as well as the circle after Floquet transformation are spreading and their shape deviates strongly from the expected one. From this amplitude, the trajectories in phase space and in Floquet space continue to spread and deviate more and more from the elliptical and circular shape.

For very large amplitudes, the triangular shape in the Floquet space disappears because of the spread and the ellipse in phase space becomes very thick (Fig. 28 and 29).

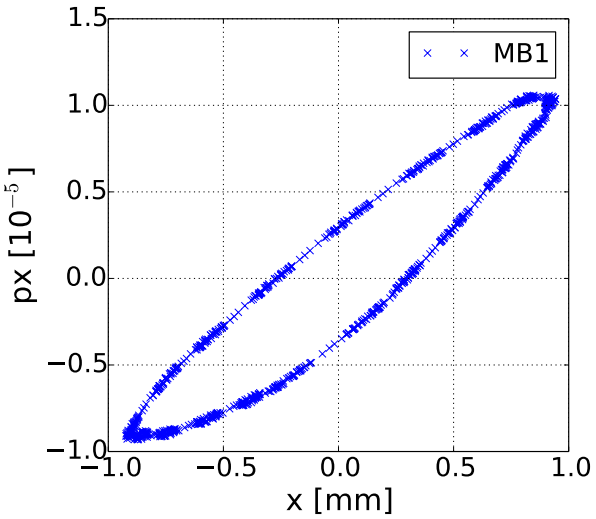

Figure 24: Poincarré section in horizontal plane at bending magnet MB1 of particle of amplitude $8.3\sigma_x$ for head-on & long-range interactions

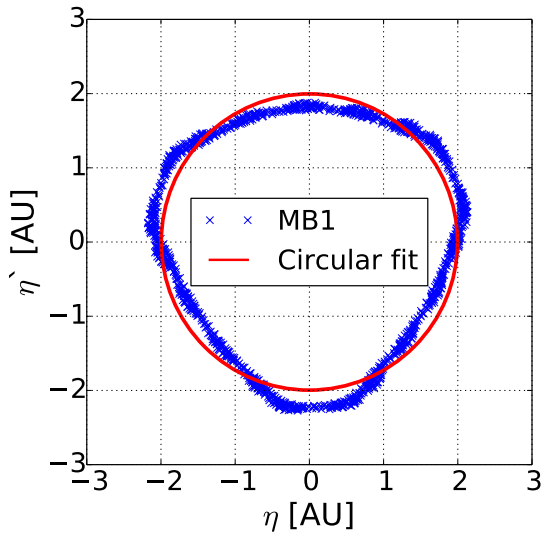

Figure 25: Floquet transformation of betatron oscillations from Fig. 24 using SVD

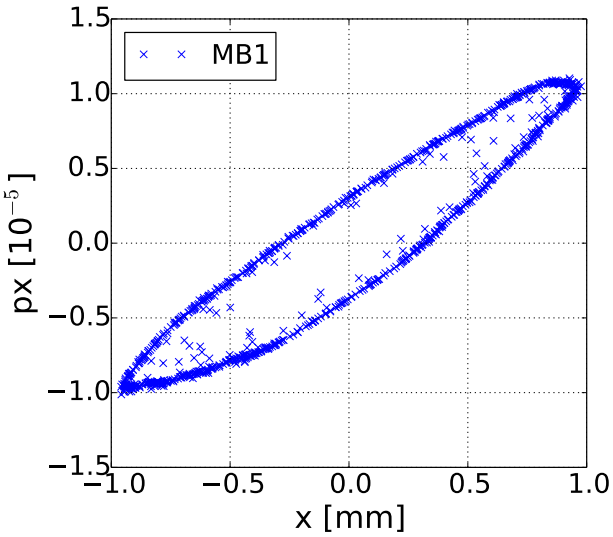

Figure 26: Poincarré section in horizontal plane at bending magnet MB1 of particle of amplitude $8.45\sigma_x$ for head-on & long-range interactions

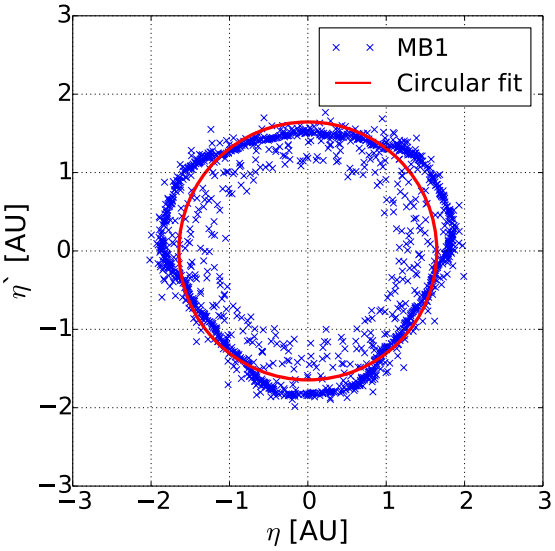

Figure 27: Floquet transformation of betatron oscillations from Fig. 26 using SVD

Finally, the α-function has also been extracted thanks to the SVD procedure. The results for the four bending magnets are presented in Fig. 30 and 31. As one can see, the curves are relatively similar to the ones for the β-beating with long-range interactions. Fig. 31 shows that the differences against the expected values (i.e. $\alpha_x \rightarrow \alpha_{x,0}$ at $12\sigma_x$ and $\alpha_x \rightarrow \alpha_{twiss}$ at $0.05\sigma_x$ taken as in head-on collisions) are very different for the smallest/largest amplitude. At $0.05\sigma_x$, the difference is very small : it remains under 0.01% which is consistent with the predictions and at $12\sigma_x$, the difference is much more important. Note that a logarithmic scale has been used in Fig. 31 because of the different scales of the deviations between $12\sigma_x$

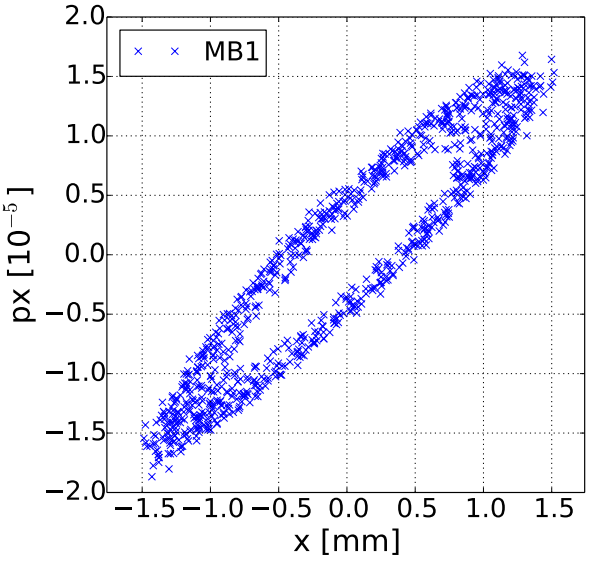

Figure 28: Poincarré section in horizontal plane at bending magnet MB1 of particle of amplitude $12\sigma_x$ for head-on & long-range interactions

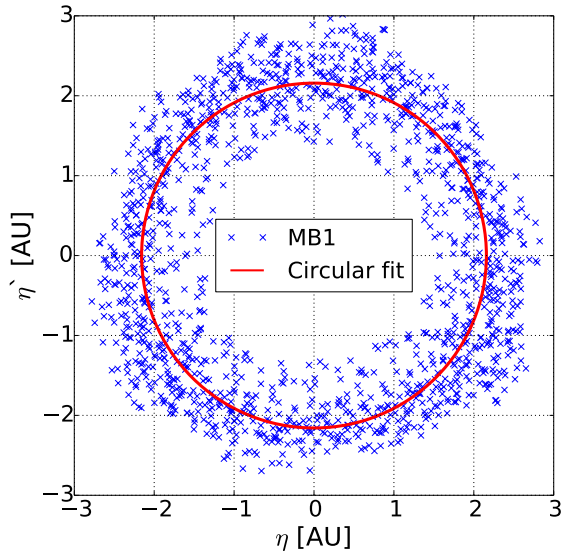

Figure 29: Floquet transformation of betatron oscillations from Fig. 28 using SVD

and $0.05\sigma_x$. The explanations concerning the chaotic behaviour from 8.3σ are the same as for the β-beating above.

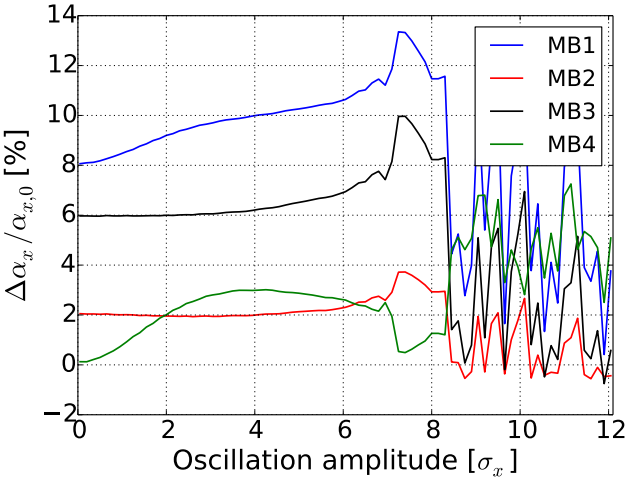

Figure 30: α-beating of a particle as a function of its oscillation amplitude at the four bending magnets for head-on & long-range interactions

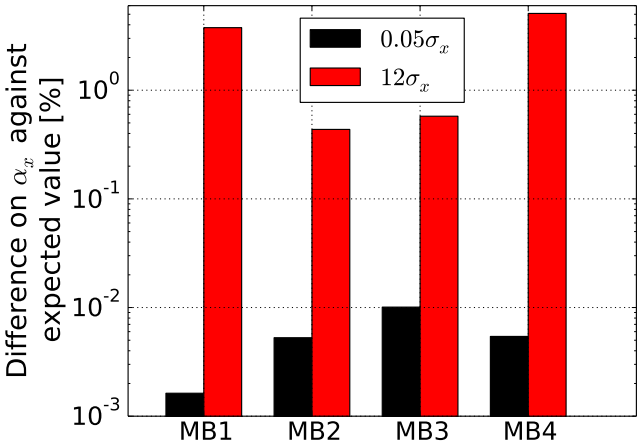

Figure 31: Difference on α_x against the expected value at $0.05\sigma_x$ and $12\sigma_x$ from Fig. 30

4 Conclusion

The effect of the phase advance between the interaction points on the β-function has been investigated and showed that the maximum of the β-beating can be adjusted by varying the phase advance between the interaction points. The simulations also revealed that the maximum of the β-beating on a given plane could be very different from one side of the ring to the other which should be taken into account in the design phase, for example of the collimation system.

The SVD procedure aiming to extract the value of the α-function and β-function thanks to Floquet transformations has been used with tracking simulations and provided workable outcomes for head-on interactions for particle oscillating at any amplitude. However, strong non-linearities from long-range interactions revealed a chaotic motion for particles with amplitude larger than 8.3σ showing the limits of this method.

The non-linear motion of particles in an accelerator is a very rich field of study. One could for example carry out the same simulations with amplitudes along the x-axis and y-axis and see if, in this case, the effects with head-on and/or long-range interactions are similar to the results found here. The range of the amplitude of the particles could also be increased so that the results for the optics and the footprint could be compared to theoretical expectations at extreme values of the amplitude.

References

[1] CERN Accelerator School - *Intermediate accelerator physics*, D. Brandt, CERN, Geneva, 2006.

[2] Wiedemann Helmut - *Particle Accelerator Physics*, Fourth Edition, Springer, 2015.

[3] Wu Chao Alexander, Tigner Maury - *Handbook of Accelerator Physics and Engineering*, World Scientific, 1999.

[4] Haruo Yanai, Kei Takeuchi, Yoshio Takane - *Projection Matrices, Generalized Inverse Matrices, and Singular Value Decomposition*, Springer, 2011.

[5] L. Rivkin, Introduction to Particle Accelerator course - *Linear Optics*, EPFL, 2015.

[6] Patrik Gonçalves Jorge - *Computation of Linear Optics Distortions due to Head-on Beam-Beam Interactions in Hadron Colliders*, CERN, 2015.

[7] Iselin F. Christophe - *The MAD Program, Physical Methods Manual*, CERN, Geneva, 1994.